Magnetoelectric transport and quantum interference effect in ultrathin manganite films

Cong Wang, Kui-juan Jin, Lin Gu, Hui-bin Lu, Shan-ming Li, Wen-jia Zhou, Rui-qiang Zhao, Hai-zhong Guo, Meng He, and Guo-zhen Yang

Citation: Applied Physics Letters **104**, 162405 (2014); doi: 10.1063/1.4873337
View online: http://dx.doi.org/10.1063/1.4873337
View Table of Contents: http://scitation.aip.org/content/aip/journal/apl/104/16?ver=pdfcov
Published by the AIP Publishing

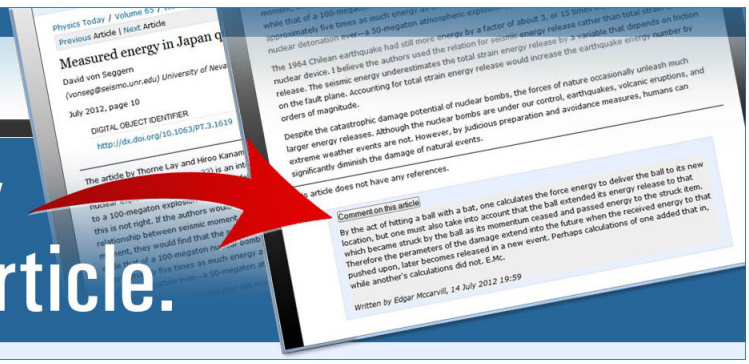

Magnetoelectric transport and quantum interference effect in ultrathin manganite films

Cong Wang, Kui-juan Jin,[a] Lin Gu, Hui-bin Lu, Shan-ming Li, Wen-jia Zhou, Rui-qiang Zhao, Hai-zhong Guo, Meng He, and Guo-zhen Yang
Beijing National Laboratory for Condensed Matter Physics, Institute of Physics, Chinese Academy of Sciences, Beijing 100190, China

(Received 7 November 2013; accepted 14 April 2014; published online 23 April 2014)

The magnetoelectric transport behavior with respect to the thicknesses of ultrathin $La_{0.9}Sr_{0.1}MnO_3$ films is investigated in detail. The metal-insulator phase transition, which has never been observed in bulk $La_{0.9}Sr_{0.1}MnO_3$, is found in ultrathin films with thicknesses larger than 6 unit cells. Low-temperature resistivity minima appeared in films with thicknesses less than 10 unit cells. This is attributed to the presence of quantum interference effects. These data suggest that the influence of the weak localization becomes much pronounced as the film thickness decreases from 16 to 8 unit cells. © *2014 AIP Publishing LLC*. [http://dx.doi.org/10.1063/1.4873337]

Advances in the investigation of complex oxide heterostructures and interfaces have been promoted by continuously improving growth and detection techniques.[1–4] The discontinuity of the crystal structures and electric field at the interface of complex oxides bring about interesting theoretical issues and experimental phenomena, such as the emergence of a high-mobility two-dimensional electron gas at the interface of two insulators[5] and the appearance of ferromagnetism at the interface of two non-ferromagnetic materials.[6] Possessing the properties of magnetism, colossal magnetoresistance (CMR), and half-metallicity,[7,8] doped manganite is more interesting when it is in two dimensional form. For the application of doped manganite, one key aspect is the magnetotransport behavior that influences their performance in magnetic tunneling junctions based on manganite films.[9] In particular, the presence of magnetic and electric dead layers has attracted much attention though their physical origin is still unknown.[10–12] In this work, we investigated the structure and magnetotransport behavior with respect to the thicknesses of ultrathin $La_{0.9}Sr_{0.1}MnO_3$ (LSMO) films. Metal-insulator phase transitions, which have never been observed in bulk LSMO, were found in ultrathin films of thickness larger than 6 unit cells (uc). Low-temperature resistivity minima appeared in the films with thicknesses less than 10 uc. This is attributed to the stronger effect of the quantum interference in ultrathin films. Through analyzing these data, we can further understand the transport properties in the framework of the interface effects and the restrained out-of-plane dimension in ultrathin manganite films.

The growth of $La_{0.9}Sr_{0.1}MnO_3$ epitaxial films on single-crystalline $SrTiO_3$ (001) (STO) substrates were carried out by a laser molecular beam epitaxy (LMBE) system with an *in situ* reflective high energy electron diffraction monitor. Detailed growth conditions and structure analysis have been reported in our previous work.[13] The as-grown films were annealed in oxygen atmosphere at 900 °C for 4 h to complement oxygen vacancies formed during deposition. The crystal structures of the as-grown and annealed films were identified by high-resolution Synchrotron X-ray diffractometry using the BL14B1 beam line of Shanghai Synchrotron Radiation Facility (SSRF). As shown in Fig. 1, the results from the synchrotron-based X-ray diffraction (SXRD) show that the *c*-axis lattice constant of the as-grown films decreases from 4.003 to 3.928 Å, while the *c*-axis lattice constant of the annealed films decreases from 3.859 to 3.833 Å when the film thickness decreases from 200 to 10 uc. The concentration of oxygen vacancies and their crucial influence on the structural and magnetic properties of the LSMO films have been thoroughly discussed previously.[13]

Figure 2 shows the high-angle annular-dark-field (HAADF) and annular-bright-field (ABF) micrographs of the as-grown and annealed LSMO films using an ARM-200F (JEOL, Tokyo, Japan) scanning transmission electron microscope (STEM) operated at 200 kV with a CEOS Cs corrector (CEOS GmbH, Heidelberg, Germany) to cope with the probe-forming objective spherical aberration. The attainable resolution in ABF images is better than 80 pm. This resolves individual oxygen atomic column with an illumination semi-angle of 25 mrad and the corresponding collection angle of 12–25 mrad. Since the HAADF contrast is proportional to 1.7th power of the atomic number; the different contrast of La and Sr provides exact chemical information and location of the interface. Moreover, the contrast of ABF micrograph is proportional to $Z^{1/3}$ and is extremely sensitive to light atoms, so oxygen vacancies can be detected at atomic scale,[13–15] which is very difficult to achieve by other methods. Good epitaxy and sharp interfaces of both the as-grown and annealed LSMO films can be readily seen from the corresponding line profile. The abrupt contrast at the interface reveals undetectable intermixing in these samples. The variation of *c*-axis lattice constants of both the as-grown and annealed LSMO films is also confirmed by STEM images. The lattice constant of the annealed film is much smaller than that of the as-grown film. Since it was revealed that *c*-axis lattice constant varied with the variation of oxygen content in manganite films,[16,17] the annealing treatment we performed can greatly reduce oxygen vacancies in the as-grown films, leading to a contraction of the lattice of LSMO films. The *c*-axis lattice constants of the as-grown

[a]Author to whom correspondence should be addressed. Electronic mail: kjjin@iphy.ac.cn

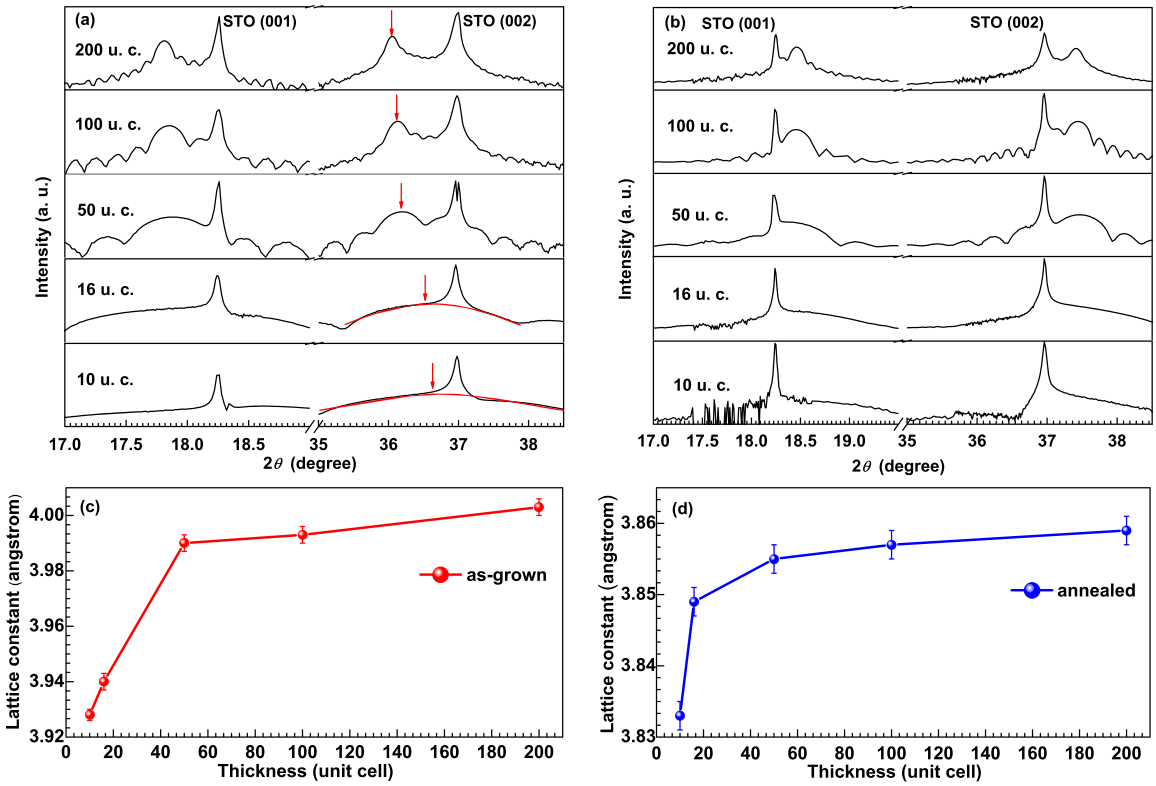

FIG. 1. SXRD patterns of the as-grown (a) and annealed (b) LSMO films with thicknesses of 200, 100, 50, 16, and 10 uc. The red arrows in (a) point at the (002) diffraction peaks of the LSMO films. The red curves in (a) are Gaussian fitting curves of the (002) diffraction peaks of the LSMO films with thicknesses of 16 and 10 uc. Thickness-dependent *c*-axis lattice constants of the as-grown (c) and annealed (d) LSMO films are deduced from the SXRD data.

and annealed LSMO films both decrease when the film thickness drops from 200 uc to 10 uc. This is unlikely the consequence of the epitaxial strain from STO substrates, because the lattice constant of the as-grown film is larger than that of STO substrates while the lattice constant of the annealed film is smaller than that of STO substrates. In our previous study,[13] ABF images show that oxygen vacancies existing around surfaces are much more than those close to interfaces. We have attributed this distribution of oxygen vacancies to the extraction of oxygen from STO substrates around the interfaces. Oxygen vacancies in thinner films are more likely to be filled up since they are closer to the interfaces and substrates. Therefore, the decrease of *c*-axis lattice constant with decreasing thickness should be attributed to less oxygen vacancies in thinner LSMO films.

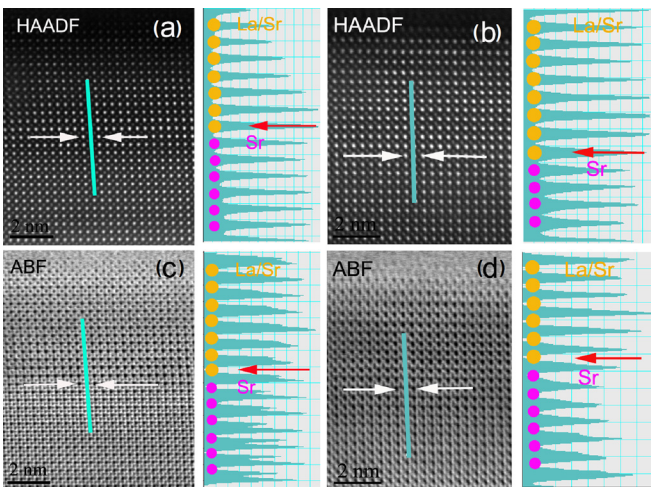

FIG. 2. (a) HAADF and (c) ABF micrographs of the as-grown LSMO film with thickness of 16 uc taken by an aberration-corrected STEM. The different contrast of La and Sr provides exact chemical information and location of the interface indicated by the white and red arrows. (b) HAADF and (d) ABF micrographs of the annealed LSMO film with thickness of 16 uc.

The in-plane lattice constants can also be extracted from STEM images of the as-grown and annealed LSMO films. From the comparison of the STEM images of the films with thickness of 16 uc, the in-plane lattice constant of the as-grown film varies from 4.08 Å to 3.91 Å from near the surface to around the interface, while that of the annealed film remains 3.91 Å with undetectable variation. These results indicate that the decrease of oxygen vacancies caused by annealing can reduce both the out-of-plane and in-plane lattice constants, and the entire lattice consequently. Moreover, the variation of the in-plane lattice constant of the as-grown film can be well explained by the distribution of oxygen vacancies revealed by our previous work.[13] Therefore, the almost invariant in-plane lattice constant of the annealed film demonstrates that oxygen vacancies near the surface was filled up to a great extent by annealing. Unlike the out-of-plane lattice constant, the in-plane lattice constant shows little change as the film thickness varies, which means the influence of epitaxial strain on the in-plane lattice constant is much smaller than that of oxygen vacancies.

Electrical measurements of the annealed LSMO films with thicknesses varying from 16 to 6 uc were carried out by a physical property measurement system (PPMS) (Quantum design). In Fig. 3(a), it is clearly seen that our annealed ultrathin films exhibit metallic conduction below the metal-

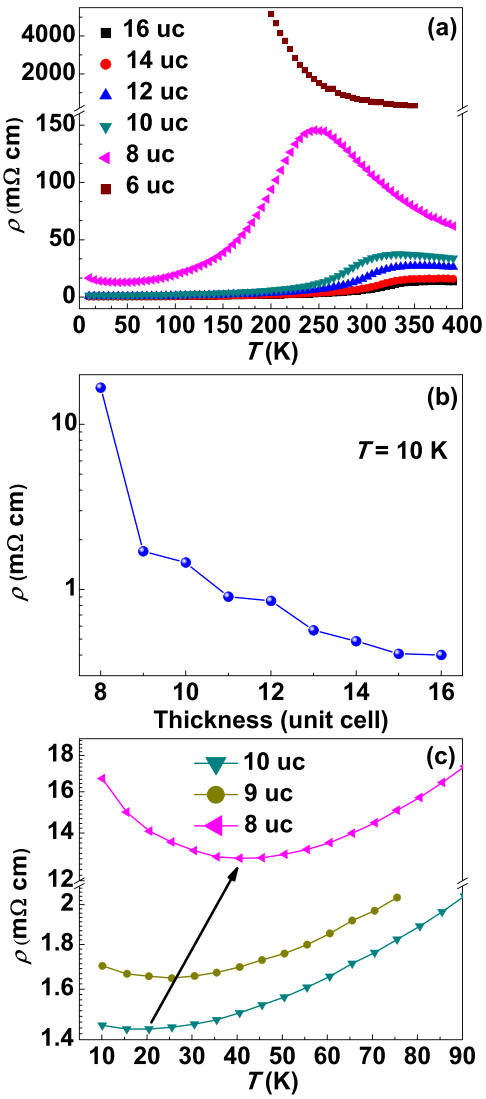

FIG. 3. (a) Temperature-dependent resistivity of the annealed films with thicknesses varying from 16 to 6 uc. (b) Thickness-dependent resistivity at 10 K of the annealed films. (c) Temperature-dependent resistivity of the annealed films with thicknesses varying from 10 to 8 uc under low temperature. The arrow indicates variation of the resistivity minimum.

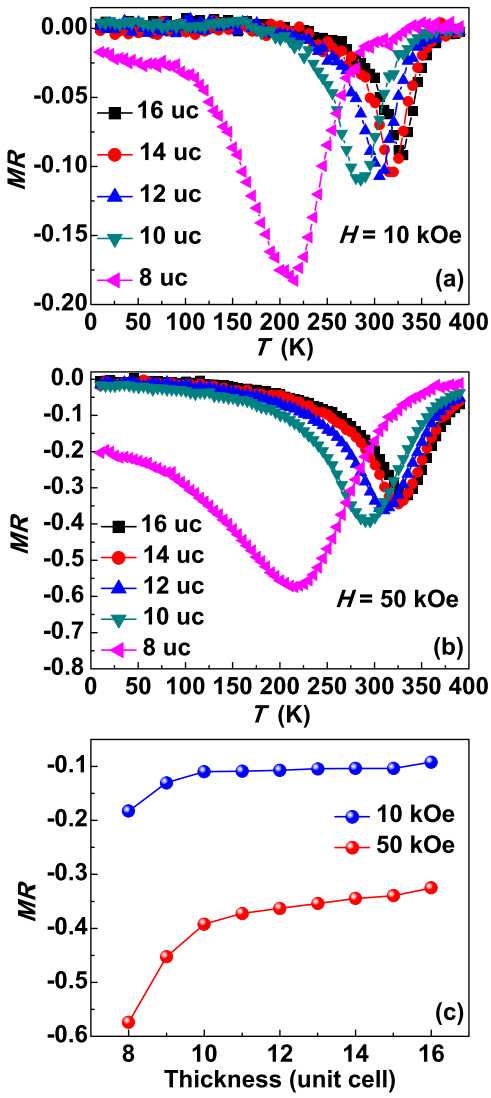

FIG. 4. (a) Temperature-dependent magnetoresistance under a magnetic field of 10 kOe of the annealed films with thicknesses varying from 16 to 8 uc. (b) Temperature-dependent magnetoresistance under a magnetic field of 50 kOe of the annealed films with thicknesses varying from 16 to 8 uc. (c) Maximum of magnetoresistance of the annealed films with thicknesses varying from 16 to 8 uc.

insulator transition (MIT) temperatures, which is quite different from the insulating conduction of bulk LSMO with a Sr doping level of 0.1 mole ratio.[18] The MIT temperature of the annealed LSMO films decreases while the resistivity increases rapidly when the film thickness decreases from 16 to 8 uc (Fig. 3(b)). In accordance with the variation of magnetic Curie temperature of the annealed LSMO films in Ref. 13, the transition temperature from ferromagnetic metallic to paramagnetic insulating phases can reach as high as 320 K, showing great potential in room-temperature application. The variation of the MIT temperature is due to the increasing influence of the interface with decreasing film thickness on the compressive epitaxial strain of the films lattice by the substrate.[19] The metallic phase and a MIT are present in films with thickness as low as 8 uc, but the resistivity of the ultrathin film with the thickness of 6 uc increases dramatically beyond the detection limit of PPMS when the temperature drops down to 200 K, corresponding to the fact that no detectable sign of the ferromagnetic metallic phase is present at this thickness.[13]

Furthermore, for LSMO films with thicknesses less than 10 uc, the resistivities reach unusual minima below 50 K (Fig. 3(c)). The existence of low-temperature resistivity minima in manganites has been observed by several groups, which was interpreted in terms of the quantum interference effect (QIE).[20–22] The QIE has two different sources: (1) electron-electron (*e-e*) interactions and (2) weak localization.[23] It was pointed out that these two sources may both act in high-quality manganites: for thick films and bulk material that behave like three-dimensional electron systems, the *e-e* interactions are more likely to dominate; for thin films that behave like two-dimensional electron systems, the weak localization is more likely to dominate.[22] The temperature of the resistivity minimum increases with decreasing thickness from 10 to 8 uc in Fig. 3(c), which means the QIE is more remarkable in thinner LSMO films.

To clarify the two sources of the QIE in our films, magnetoresistance (MR) measurements with the magnetic field

perpendicular to the film surfaces were taken. The *MR* is defined as

$$MR = \frac{R_H - R_0}{R_0}, \quad (1)$$

in which R_H is the resistivity under the magnetic field of H, and R_0 is the zero-field resistivity. As shown in Fig. 4, the absolute peak value of *MR*, under the magnetic field of 10 kOe and 50 kOe, respectively, becomes large when the film thicknesses decrease from 16 to 8 uc. For the thinnest LSMO films with the thickness of 8 uc, the low-temperature negative *MR* is quite remarkable compared to the thicker films. Noticing that the low-temperature *MR* would be positive for spin splitting and orbital effects if *e-e* interactions dominate, it seems that the magnetic field suppression of weak localization is responsible for the negative MR in our annealed LSMO ultrathin films.[22] Thus, as the film thickness of the annealed LSMO films decreases from 16 to 8 uc, the influence of the weak localization becomes much pronounced.

In conclusion, we systematically studied the structural and magnetotransport properties of LSMO ultrathin films with thicknesses varying from 16 to 6 uc. Good epitaxy and sharp interfaces are indicated by STEM. Along with the ferromagnetic-paramagnetic phase transition, the metal-insulator transition, which cannot be observed in bulk LSMO, emerges in the annealed ultrathin films as the thickness drops down to 8 uc (about 3.2 nm). Furthermore, the low-temperature resistivity minima appear in the LSMO films with thicknesses less than 10 uc. This is attributed to the stronger effect of the quantum interference in thinner films. Our results indicate that the intriguing transport properties of the ultrathin LSMO films are strongly affected by the restrained out-of-plane dimension, and that the influence of the weak localization becomes much pronounced as the film thickness of the annealed LSMO films decreases from 16 to 8 uc. This could be further exploited for devices based on ultrathin films of perovskite-type oxides.

This work was supported by the National Basic Research Program of China (No. 2012CB921403) and the National Natural Science Foundation of China (Nos. 10825418, 11134012, and 11004238). The XRD measurement was supported by the Shanghai Synchrotron Radiation Facility (SSRF).

[1]D. G. Schlom, L. Q. Chen, X. Q. Pan, A. Schmehl, and M. A. Zurbuchen, J. Am. Ceram. Soc. **91**, 2429 (2008).
[2]K. J. Jin, H. B. Lu, K. Zhao, C. Ge, M. He, and G. Z. Yang, Adv. Mater. **21**, 4636 (2009).
[3]J. Mannhart and D. G. Schlom, Science **327**, 1607 (2010).
[4]M. Bibes, J. E. Villegas, and A. Barthelemy, Adv. Phys. **60**, 5 (2011).
[5]A. Ohtomo and H. Y. Hwang, Nature **427**, 423 (2004).
[6]T. Koida, M. Lippmaa, T. Fukumura, K. Itaka, Y. Matsumoto, M. Kawasaki, and H. Koinuma, Phys. Rev. B **66**, 144418 (2002).
[7]I. Zutic, J. Fabian, and S. D. Sarma, Rev. Mod. Phys.**76**, 323 (2004).
[8]M. Bibes and A. Barthelemy, IEEE Trans. Electron Devices **54**, 1003 (2007).
[9]S. Valencia, Z. Konstantinovic, D. Schmitz, A. Gaupp, LI. Balcells, and B. Martínez, Phys. Rev. B **84**, 024413 (2011).
[10]J. Z. Sun, D. W. Abraham, R. A. Rao, and C. B. Eom, Appl. Phys. Lett. **74**, 3017 (1999).
[11]R. P. Borges, W. Guichard, J. G. Lunney, J. M. D. Coey, and F. Ott, J. Appl. Phys. **89**, 3868 (2001).
[12]M. Bibes, S. Valencia, LI. Balcells, B. Martínez, J. Fontcuberta, M. Wojcik, S. Nadolski, and E. Jedryka, Phys. Rev. B **66**, 134416 (2002).
[13]C. Wang, K. J. Jin, L. Gu, H. B. Lu, S. M. Li, W. J. Zhou, R. Q. Zhao, H. Z. Guo, M. He, and G. Z. Yang, Appl. Phys. Lett. **102**, 252401 (2013).
[14]C. L. Jia and K. Urban, Science **303**, 2001 (2004).
[15]O. L. Krivanek, F. C. Matthew, N. Valeria, J. P. Timothy, J. C. George, D. Niklas, S. O. Christopher, S. S. Zoltan, P. O. Mark, T. P. Sokrates, and J. P. Stephen, Nature **464**, 571 (2010)
[16]Z. T. Xu, K. J. Jin, L. Gu, Y. L. Jin, C. Ge, C. Wang, H. Z. Guo, H. B. Lu, R. Q. Zhao, and G. Z. Yang, Small **8**, 1279 (2012)
[17]P. Orgiani, A. Y. Petrov, R. Ciancio, A. Galdi, L. Maritato, and B. A. Davidson, Appl. Phys. Lett. **100**, 042404 (2012).
[18]A. M. H. Gosnet and J. P. Renard, J. Phys. D: Appl. Phys. **36**, R127 (2003).
[19]F. S. Razavi, G. Gross, H. U. Habermeier, O. Lebedev, S. Amelinckx, G. Van Tendeloo, and A. Vigliante, Appl. Phys. Lett. **76**, 155 (2000).
[20]D. Kumar, J. Sankar, J. Narayan, R. K. Singh, and A. K. Majumdar, Phys. Rev. B **65**, 094407 (2002).
[21]M. Ziese, Phys. Rev. B **68**, 132411 (2003).
[22]L. Maritato, C. Adamo, C. Barone, G. M. De Luca, A. Galdi, P. Orgiani, and A. Y. Petrov, Phys. Rev. B **73**, 094456 (2006).
[23]P. A. Lee and T. V. Ramakrishnan, Rev. Mod. Phys. **57**, 287 (1985).